Vector Magnetization Model

by Ali Jamali

B.Sc. in Electrical Engineering, June 2003, Tehran University, Iran
M.Sc. in Electrical Engineering, May 2013, The George Washington University, USA

A Dissertation submitted to

The Faculty of
The School of Engineering and Applied Science
of The George Washington University
in partial fulfillment of the requirements
for the degree of Doctor of Philosophy

May 20, 2018

Dissertation directed by

Edward Della Torre
IEEE Life Fellow and Professor of Engineering and Applied Science

The School of Engineering and Applied Science of The George Washington University certifies that Ali Jamali has passed the Final Examination for the degree of Doctor of Philosophy as of date of dissertation defense. This is the final and approved form of the dissertation.

Vector Magnetization Model

Ali Jamali

Dissertation Research Committee:

Edward Della Torre, Professor of Engineering and Applied Science, Dissertation Director

Shahrokh Ahmadi, Teaching Professor in Electrical Engineering, Committee member

David Nagel, Research Professor of Engineering and Applied Science, Committee Member

Payman Dehghanian, Assistant Professor of Electrical Power and Energy, Committee Member

Amir Aslani, Manager, ECE Laboratory, Committee Member

© Copyright 2018 by Ali Jamali
All rights reserved

Dedication

To my wife, Zeinab Golabkesh.

Abstract of Dissertation

Vector Magnetization Model

In hysteresis modeling, we predict magnetization as a function of the applied field and magnetic state. Most hysteresis models are scalar. A scalar model assumes that only the magnitude of the applied field changes and therefore the direction of the magnetization is always along the direction of the applied filed. In this dissertation, I assumed the magnitude of the applied field is constant and we rotate the magnetization. I developed a vector model that can successfully predict the direction of the magnetization. The idea of decomposing magnetization into reversible and irreversible components is introduced in chapter 2 of the dissertation. In chapter 3, I developed the model for uniaxial media by using Stoner-Wohlfarth model for the direction of reversible component. This has been done in chapter 4 by assuming anisotropy field is parallel with easy axis as another variation of the model. These two has been compared in chapter 4. In chapter 5, I generalized the idea to the cubic particles. I also showed and proved a graphical visualization of the Stoner-Wohlfarth model. Finally, in chapter 6, I showed how we can improve the model by taking averages over orientation of hysteron's easy axes.

Table of Contents

Dedication iv

Abstract of Dissertation v

Table of Contents vi

List of Figures ix

Chapter 1: Introduction 1

Chapter 2: Vector Properties of Magnetostriction 4

2.1 Overview 4

2.2 Two Isotropic Media 5

2.3 Simulation and experimental results 7

2.4 Conclusion 10

Chapter 3: Vector Magnetization of a Distribution of Uniaxial Particles 11

3.1 Background 11

3.2 Overview 12

3.3 Energy approach 12

3.4 Model Algorithm 13

3.5 Magnetization Oscillation 14

3.6 Magnetization Rotation 16

3.7 Bifuraction Curve 18

3.8 Simulation and Experimental Results 19

3.9 Conclusion 21

Chapter 4: A Vector Model for Off-Axis Hysteresis Using Anisotropy Field 23

4.1 background 23

4.2 overview 25

4.3 Gibb's Free Energy Function.....26

4.4 Oscillation and Rotational Modes.....27

4.5 Bifurcation Curve.....31

4.6 Unitary Magnetization.....33

4.7 Conclusion.....34

Chapter 5: Vector magnetization of a distribution of cubic particles.....36

5.1 Background.....36

5.2 Overview 37

5.3 Energy Approach.....37

5.4 Direction of The Anisotropy Field 39

5.5 Simulation and Experimental Results 41

5.6 Conclusion 44

Chapter 6: Properties of Uniaxial Media Model.....46

6.1 Background 46

6.2 Model behavior.....47

6.3 Hangle-mangle curves.....51

6.4 Standard tests.....52

6.5 Averaging over orientation 54

6.6 Conclusion.....57

Chapter 7: Summery, Conclusion and Future Researches.....58

References.....**60**

List of Figures

Fig. 1. Decomposition of the magnetization M into a reversible component, Mr, and an irreversible component, Mi…….…….....……5

Fig. 2. Typical critical surfaces of hysterons of (a) native and (b) polycrystalline isotropic media. In (a) a rotating field will not cross the hysteron's critical surface. In (b) a rotating field will cross some critical surfaces causing the magnetization to lag the magnetic field……...…6

Fig. 3. A theoretical plot of the angle (Lag Angle) by which the magnetization, M, lags the rotating magnetic field, H. The Lag Angle decreases as the rotating field magnitude increases……..…….……..8

Fig. 4. Angle of magnetization trajectory (θM) as a function of angle of sample rotation (θ) for fixed fields of -1000 G (red triangles) and +1000 G (blue circles). Insets: Zoomed graphs……...8

Fig. 5. A graphical realization of the model……..14

Fig. 6. Reversible magnetization angle (θ_R) vs applied field angle (θ_H) in oscillation mode (h < 0.5). The dashed line represents the locus of maximum θ_R……15

Fig. 7. Reversible magnetization angle (θ_R) vs applied field angle (θ_H) in rotation.…….16

Fig .8. Hysteresis behavior of Reversible magnetizationangle……..17

Fig.9. Reversible magnetization angle (θ_R) vs applied field angle (θ_H) for h >1……...17

Fig. 10. Bifurcation curve together with two circles of h=0.5 and h=1……19

Fig. 11. Total magnetization angle (θ_M) vs applied field angle (θ_H)……..20

Fig.12. Measurment of total magnetization angle (θ_M) vs applied field angle (θ_H) for a sample of magnetic tape showing oscillation and rotation modes……21

Fig. 13. Graphical realization of the model…….....…….....25

Fig. 14. Comparison between reversible magnetization versus applied field…….....29

Fig. 15. Behavior of (a) the Stoner-Wohlfarth model and (b) the anisotropy field model in the rotational mode of magnetization……30

Fig. 16. Unitary magnetization……..33

Fig.17. Visualization of the Stoner-Wohlfarth model.....40

Fig.18. Graphical realization of the total magnetization for cubic anisotropy field……..42

Fig.19. Lag angle curves for two different applied field magnitudes in rotation……..43

Fig.20. Cubic particle's magnetization trajectory for 360^{o} rotating field……..43

Fig. 21. Errorfunction approximation of the major loop and first order reversal……..48

Fig.22: Magnetization (solid), applied field (dashed)……50

Fig. 23. Location of position of change from lag to lead……...51

Fig. 24. Hangle-mangle curves for parameters……..53

Fig.25. Unitary magnetization with (right) and without (left) averaging.....55

Fig.26. Lag angle curve with (right) and without (left) averaging……56

Chapter 1: Introduction

Magnetism has a vector nature which is not reflected in current scalar models. I developed a new non-linear vector magnetization model that can be used for a better understanding of magnetic behavior. Scalar models of magnetization discuss processes in which the magnetization is measured and modeled along the axis of field variations. In certain applications, applied fields are not along the reference axis of the sample, or are rotating. In such cases, the magnetization might not be in the same direction of the applied field. In previous works, finite elements codes (FEM) as a linear method were employed for this modeling purpose [DEL,2014].

The three dimensional shapes of the sample means that the different parts of the magnetization points in different directions, which makes it complicated and nearly impossible to be analyzed correctly by the existing models, such as FEM and scalar Preisach. Currently, a vector model of hysteresis does not exist. We are developing such a model and have made substantial progress [DEL, 2015] to obtain a new 3-D Preisach model, and test it by simulation, analysis and experiment.

We can think of a scalar model as process in which all the field variations lie along a single axis and we are interested only in the component of magnetization along that axis. In a real magnetizing process, besides changing its value, the applied field could rotate. Furthermore, especially if the material is anisotropic, the resulting magnetization might not be in the same direction as the applied field. Thus, it is necessary to characterize material behavior in two or more dimensions.

A real-world application of this model is developing magnetic devices and sensors,

drug delivery systems and nondestructively evaluating stresses and fatigues, and predicting the magnetic signature of nano-particles used in small actuators.

In this dissertation, I developed a vector magnetization model for uniaxial media. In this model, magnetization is vector sum of reversible and irreversible components. We need direction and magnitude of irreversible and reversible components to be able to derive total magnetization vector. We treat the irreversible magnetization same way we deal with magnetization in scalar models, therefore, scalar Preisach model is used for magnitude of irreversible component and its direction is always along easy axis. The reversible component changes by Stoner-Wohlfarth model. One assumption in chapters 4 ,5 and 6 is that the model is developed for behavior of the perfectly aligned hysteron. This assumption has been removed for chapter 7. In chapter 6, a 3D model is presented for an assembly of hysterons as a generalization of the Stoner-Wohlfarth model. The decomposition of magnetization into an irreversible component, $\mathbf{M_I}$, and a reversible component, $\mathbf{M_R}$ is unique. We assumed that $\mathbf{M_I}$ is a function only of the applied field. The magnetic state of the system is the contribution to $\mathbf{M_I}$ as a function of the critical field of the hysteron. The critical field of the hysteron depends on the orientation of the applied field.

Reversible magnetization, $\mathbf{M_R}$, is a function of the magnetic state as well as the applied field. The magnitude of $\mathbf{M_R}$ is calculated by some arctangent or exponential function. The direction of $\mathbf{M_R}$ is determined by minimizing sum of the magnetocrystalline uniaxial anisotropy energy and the Zeeman energy (chapter 4) or by assuming that anisotropy field is parallel with easy axis (chapter 5).

The idea is also generalized to create a model for the vector magnetization of a distribution of particles with cubic anisotropy. The model is extended to include cubic anisotropy

projected to the (100) plane (chapter 6). The magnitude of the irreversible component is modeled using a Preisach differential-equation approach; however, other valid models can be used. The direction of the reversible component is modeled using the minimum energy approach of the classical Stoner–Wohlfarth model and taking into account the anisotropy field. The formulation of the generalized model is derived and its results are discussed considering ,oscillation and rotational modes, lag angle, and magnetization trajectories [JAM, 2017]

Averaging over orientation have been done to improve the model(chapter7). By assuming that the distribution of critical fields is Gaussian, then the major loop will be an error function. For small rotating fields, the magnetization will oscillate between two extreme values on the same side of the origin. For larger fields, the irreversible magnetization can change sign and the magnetization will rotate about the origin. We start with a demagnetized specimen, then apply a field that starts along the easy axis and then rotates about the origin. For the first 90°, the magnetization will follow a circular path. Beyond that point the irreversible magnetization will start to change, and the magnetization will start to spiral in towards the origin. Therefore, we will get asymmetrical loops which can be compared with experiment. [DEL, 2017]

Chapter 2: Vector Properties of Magnetostriction

2.1 overview

The vector properties of a newly-developed Preisach-type magnetostriction model are discussed. The model uses a modified version of the Della Torre-Pinzaglia-Cardelli (DPC) model to compute the irreversible and the reversible components of the magnetization. The magnetostriction can then be simulated by assuming that its magnitude is proportional to the magnetization and its direction is dependent on the magnetization history. The modeling approach is outlined for two types of isotropic media; native and polycrystalline. The preliminary results show excellent agreement with the rotational magnetization measurements for a sample of high-strength steel.

Most computational models for magnetostriction are scalar in nature. However, magnetizing processes are inherently three-dimensional. A modified version of the Della Torre-Pinzaglia-Cardelli (DPC) model is used to simulate the vector magnetization processes1. The new model computes the magnetization as the sum of locally irreversible magnetization, **Mi**, and a reversible magnetization, **Mr**. This decomposition is unique since **Mi** is totally irreversible, so the magnetization can only change by Barkhausen jumps. **Mr** on the other hand is totally reversible as long as **Mi** does not change. Thus if the applied field is increased incrementally and then decreased, the decomposition of the magnetization is as shown in Fig. 1. It is assumed that there will be no jumps in the reverse process, however, if there are, they can be eliminated by a second process.

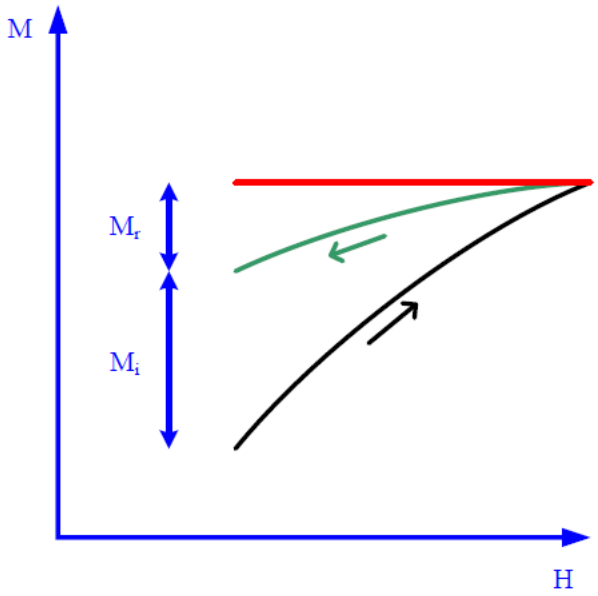

Fig.1 . Decomposition of the magnetization M into a reversible component, Mr, and an irreversible component, Mi

On further increasing the field, the irreversible magnetization experiences a jump. Then the magnetization angle will lead the applied field angle until the applied field angle reaches the easy axis. On continuation of the rotation this process will repeat itself. For an assembly of hysterons, the sharp transitions are smoothed out. Assemblies of non-uniaxial hysterons will have more than one easy axis. Consequently, in one rotation any number of jumps, and any change in magnetization, could happen.

2.2 **Two Isotropic Media**

Two types of isotropic media are considered: a native medium in which the individual

hysterons are isotropic, and a polycrystalline isotropic medium whose hysterons have a uniform angular distribution of easy axes. In the native medium the critical surface is a sphere centered on the origin. Hence in a rotating magnetic field the applied field will not cross the critical surfaces of each hysterons as seen in Fig. 2(a). The lag angle between the magnetization and the applied field will then be zero. In the polycrystalline isotropic medium, the applied field will cross the critical surface twice per revolution for each hysteron as seen in Fig. 2(b), and the magnetization will lag the applied field. For this medium, the steady state lag angle will be a constant as shown in Fig 3.

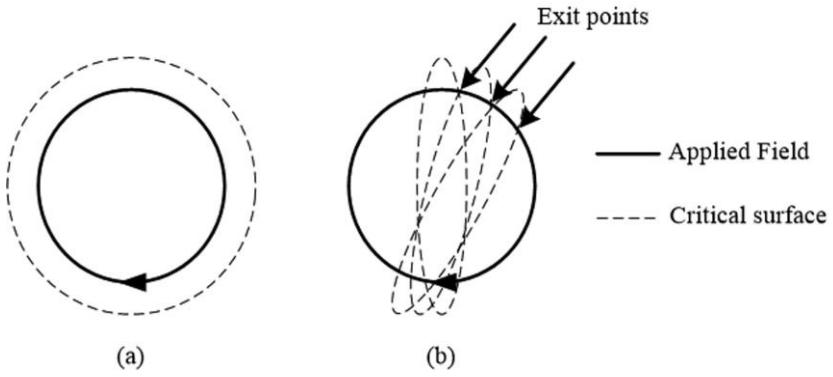

Fig. 2. Typical critical surfaces of hysterons of (a) native and (b) polycrystalline isotropic media. In (a) a rotating field will not cross the hysteron's critical surface. In (b) a rotating field will cross some critical surfaces causing the magnetization to lag the magnetic field.

In the modified DPC model, a critical surface is associated with each hysteron. Whenever the applied field exits the critical surface, the internal state switches to a unique internal state of the corresponding hysteron, unless it is already there. Otherwise, the internal state

is insensitive to the applied field. It is noted that for an isotropic hysteron, the critical surface is a sphere centered on the origin, as seen in Fig. 2(a). Under a rotating applied field the applied field will not cross the critical surface, and there will be no loss associated with this condition.

2.3 Simulation and experimental results

This modified DPC model uses the lag angle curves to determine the anisotropy of the hysterons. For a native isotropic medium, the magnetization is free to rotate. As the applied field rotates the magnetization will rotate along with a zero lag angle. For a polycrystalline isotropic medium, once the initial transients evanesce, the magnetization will lag the applied field by a constant angle. That lag angle is positive. The lag angle will decrease as the applied field is increased as shown in Fig. 3. A vector vibrating sample magnetometer measurement of the lag angle for a polycrystalline isotropic medium is shown in Fig. 4. The rotating magnetization trajectories were measured as follows: A negative saturation field of -7000 G is applied and then increased to 1000 G. The sample is then rotated clockwise in increments of 10o from a reference starting point to 360o. The polar angle (θM) of the magnetization trajectory can be computed using the two measured magnetization components. The procedure was repeated at -1000 G for sample saturated at 7000 G.

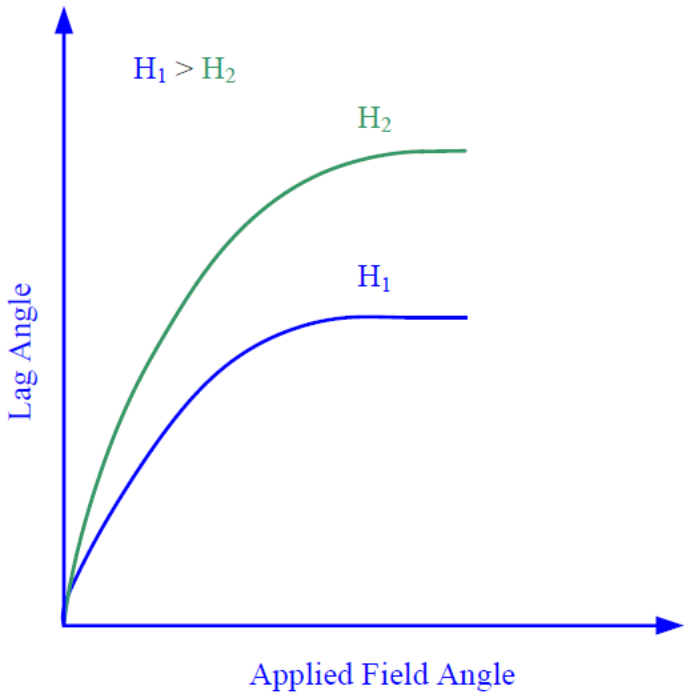

Fig. 3. A theoretical plot of the angle (Lag Angle) by which the magnetization, M, lags the rotating magnetic field, H. The Lag Angle decreases as the rotating field magnitude increases.

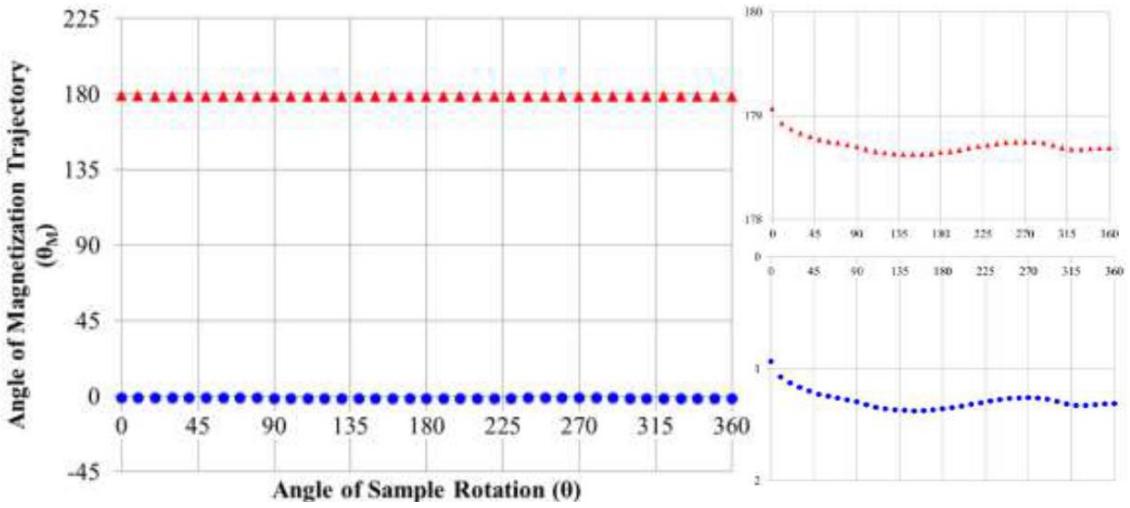

Fig. 4. Angle of magnetization trajectory (θM) as a function of angle of sample rotation (θ) for fixed fields of -1000 G (red triangles) and +1000 G (blue circles). Insets: Zoomed graphs.

The model's behavior in a rotating magnetic field is now described for a single uniaxial hysteron. All angles will be measured from the easy axis. The angle of the applied field is θH, and that of the magnetization is θM. If we begin the process with both angles equal to zero, then as the field rotates, for small fields, θM will oscillate about zero. As the field increases, eventually the irreversible magnetization will exhibit a jump and **Mr** will increase and lie along the easy axis. Since the **Mr** lies along the applied field direction, it is seen that initially $\theta M < \theta H$ and the magnetization lies between the applied field direction and the easy axis. The magnetization angle lags the applied field angle. The lag angle is defined as $\theta L = \theta M - \theta H$. For a uniaxial particle, the magnetization will lag the applied field until the field has rotated to the point that the irreversible magnetization will switch. The magnetization will rotate towards the nearest easy axis and the magnetization angle will lead the field angle. On further rotation the lag angle will decrease until the field angle (and magnetization) is again aligned with the easy axis. Continued rotation will cause an increasing lag angle. On further rotation this process repeats.

A real medium will have many hysterons with a variety of critical surfaces. This has the effect of smoothing the steps in the magnetization angle. Measurements of a real lag angle curves for a uniaxial medium are shown in [KAH,2005]. It was seen that those curves are periodic in angle with a period of 180o.

The energy dissipated in a changing magnetic field is given by:

$$E = \int_{M_1}^{M_2} \mu_0 H . dM \qquad (1)$$

Accordingly, in a rotating field, the change in magnetization is perpendicular to the magnetization. As long as **M** is in the same direction as **H**, d**M** will be perpendicular to it and no energy will be dissipated. Thus, the native isotropic medium will not dissipate energy. The artificial isotropic medium will dissipate energy directly proportionally to the sine of θL.

2.4 Conclusion

Our measurements of the effect of a transverse bias field (HT) on longitudinal magnetostriction of high-strength steel were used to discuss the physical limitations of vector magnetostriction models. The vector magnetostriction model involves two steps. First the vector magnetization is calculated using a distribution of vector hysterons. Then the magnetostriction is calculated directly from the magnetization. It assumes that the magnitude of the magnetostriction is directly proportional to the strength of the applied field and its direction is determined by the magnetization history. The preliminary results for isotropic media show excellent agreement with our rotational magnetization measurements on high-strength steel. The algorithm developed requires to be compared to the measurements of an anisotropic sample to test its robustness. The modeling efforts initiated in this chapter aim at testing the hypothesis of decoupling the modeling of magnetostriction from the hysteretic magnetic properties of materials.

Chapter 3: Vector Magnetization of a Distribution of Uniaxial Particles

3.1 Background

In this chapter, a model for the vector magnetization of a distribution of uniaxial particles is proposed. It can be thought of as a generalization of the Stoner–Wohlfarth (SW) model [STO, 1948]. The proposed model decomposes the total magnetization into unique irreversible and reversible processes. The SW model, on the other hand, models reversible magnetization only. A comprehensive review of the SW model and its limitations can be found in [TAN,2008]. A vector hysteron approach was applied to the SW model to remove some of the limitations in [PET,2011]. A generalization of the SW model for nonsingle-domain particles is introduced in [CIM,2013]. The model is developed for an idealized distribution of uniaxial particles, where all the particles are aligned along the medium's easy axis. When the applied magnetic field is zero, the magnetization vector of all the particles will lie along the easy axis. It is assumed that the particles are nanostructures that are too small to support domain walls, and hence, they are single domain. There are two modes of change in the magnetization: an irreversible mode by Barkhausen jumps and a reversible mode by magnetization rotation. The irreversible change in magnetization causes energy loss. The reversible changes are single-valued and lossless. The irreversible magnetization, MI , is only sensitive to the easy axis component of the applied field. The particles whose critical fields are exceeded will be switched to the direction of the easy axis component of the applied field. This process is irreversible and has the deletion property of the classical Preisach model [DEL,1999]. The reversible magnetization, MR, is one of rotation, so the magnitude of MR is constant and is a single-valued function of the

applied field as long as *MI* does not change. When the applied field is along the easy axis, there is no rotation of *MR* and the reversible susceptibility along the easy axis is zero. At any stage in the magnetization process, if the applied field is reduced to zero, the reversible component goes to zero, and the total magnetization measured is the irreversible component.

3.2 Overview

A model for the vector magnetization of a distribution of uniaxial particles is presented. In chapter 2, I showed how magnetization can be decomposed the magnetization into two components and modeled the total vector magnetization as their vector sum. Anisotropy could be ideally modeled as a constant field, but this leads to a model of unidirectional anisotropy. Considering uniaxial media, such approach will only be valid for small angles. Hence, in this chapter, a model is proposed that calculates the total magnetization of a distribution of uniaxial particles as the vector sum of irreversible and reversible components. The magnitude of the irreversible component is modeled using a Preisach differential-equation approach; however, other valid models can be used. The direction of the reversible component is modeled using the minimum energy approach of the classical Stoner–Wohlfarth model. The final result of the model is an unsymmetrical lag-angle plot for intermediate applied field values, which is consistent with the measurements.

3.3 Energy approach

Two components of energy are the uniaxial anisotropy energy and the Zeeman energy. Defining θ_R as the angle between M_R and the easy axis, and θ_H as the angle between the

applied field and the medium's common easy axis, then the magnetocrystalline uniaxial anisotropy energy [STO,1948] is given by $W_U = K_U \sin^2\theta_R$, such that $K_U = V * K_1$, where V is the volume of the domain and K_1 is the uniaxial magnetocrystalline anisotropy constant that depends on composition and temperature. In addition, there is anisotropy due to the demagnetization field which is related to the magnetization by the demagnetizing tensor. The Zeeman energy is $W_Z = -M_R H \cos(\theta_H - \theta_R)$, such that $M_R = V\mu_0 M_s$ where M_s is the saturation magnetization. For a distribution of hysterons, the irreversible magnetization is calculated by the classical Preisach model.

The value of θ_R as a function of θ_H can be computed by finding the minimum of $W = W_U + W_Z$ with respect to θ_R that is, $\frac{\partial W}{\partial \theta_R} = 0$. This can be simplified to the following equation:

$$\sin\theta_R \cos\theta_R - h \sin(\theta_H - \theta_R) = 0, \qquad (2)$$

where h is the applied field (H) normalized to the anisotropy field (H_K=2K$_u$/M_R).

Equation 1 describes the irreversible magnetization angle as a function of applied field angle implicitly. For large applied field, $W_Z \gg W_U$, and the minimum energy occurs at $\theta_R = \theta_H$.

3.4 Model Algorithm

Similar to the model introduced in [DEL,2015], the total magnetization, M, is the vector sum of irreversible magnetization, M_I, and reversible magnetization, M_R. The direction of M_I is along easy axis and its magnitude is computed by a differential equation approach [VAJ,1993]. The direction of M_R is determined by Eq. 2, and its magnitude is computed by a magnetization-dependent function [DEL,1999]. A Graphical realization of the model is introduced in Fig.5.

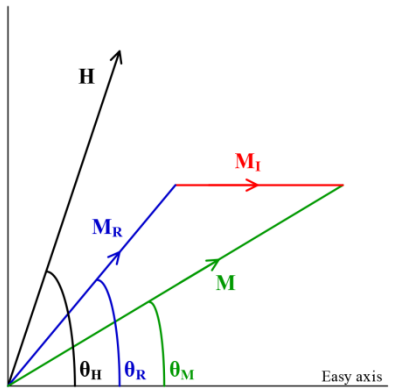

Fig. 5. A graphical realization of the model. All angles are measured from the easy axis. M_I is the irreversible magnetization, M_R and θ_R are the reversible magnetization and its angle, M and θ_M are the total magnetization and its angle, and H and θ_H are the applied field and its angle.

There are two modes of change of M_R with a rotating applied field: rotation and oscillation.

3.5 Magnetization Oscillation

Oscillation occurs when the normalized applied field, h, is less than 0.5. To mathematically derive this threshold, it can be shown that the graph of θ_R as function of θ_H reaches a maximum as long as the applied field is less than the threshold. We can simplify Eq. 2 and rewrite it as:

$$\sin\theta_H \csc\theta_R - \cos\theta_H \sec\theta_R = \frac{1}{h} \qquad (3)$$

By taking implicit derivative with respect to θ_H:

$$\frac{d\theta_R}{d\theta_H} = \frac{\cos\theta_H \csc\theta_R + \sin\theta_H \sec\theta_R}{\sin\theta_H \csc\theta_R \cot\theta_R + \cos\theta_H \sec\theta_R \tan\theta_R} = 0$$

$$\cos\theta_H \csc\theta_R + \sin\theta_H \sec\theta_R = 0$$

$$\cot\theta_R = -\tan\theta_H$$

$$\theta_R + \frac{\pi}{2} = \theta_H \qquad (4)$$

Equation 4 suggests that the maximum points of all θ_R - θ_H curves are located on a straight line that is shown in Fig.6.

By plugging (4) into (3), the following equation is obtained:

$$\sin(\theta_R + \frac{\pi}{2}) \csc\theta_R - \cos(\theta_R + \frac{\pi}{2}) \sec\theta_R = \frac{1}{h}, \qquad (5)$$

which simplifies to: $\sin(2\theta_R) = 2h$

Therefore, only for h<0.5 Eq. 1 has a maximum. This maximum would be $\theta_{R_{max}} = \frac{1}{2}\sin^{-1}(2h)$ which occurs when $\theta_H = \theta_R + \frac{\pi}{2} = \frac{\pi}{2} + \frac{1}{2}\sin^{-1}(2h)$.

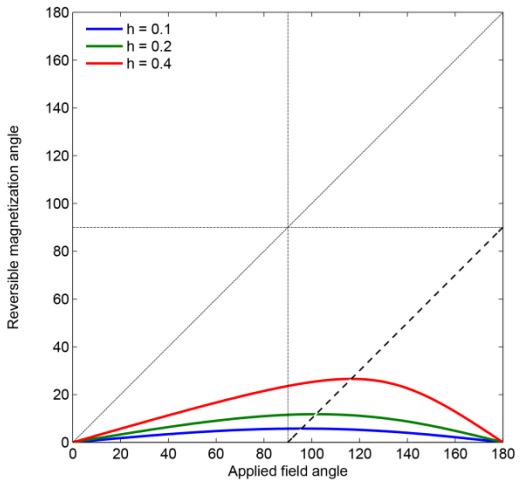

Fig. 6. Reversible magnetization angle (θ_R) vs applied field angle (θ_H) in oscillation mode (h < 0.5). The dashed line represents the locus of maximum θ_R.

3.6 Magnetization Rotation

Rotation occurs when the normalized applied field, *h*, is larger than 0.5. For the values of *h* between 0.5 and 1, for some applied field angles in the interval $(\frac{\pi}{2} - \theta_C, \frac{\pi}{2} + \theta_C)$, Eq. 2 has three solutions as shown in Fig. 7. In this case, as the applied field angle increases from 0 to $\frac{\pi}{2} + \theta_C$, the reversible magnetization angle varies on lower part of the curve and at $\theta_H = \frac{\pi}{2} + \theta_C$ it moves on the upper curve. On the other hand, when the angle decreases from π to $\frac{\pi}{2} - \theta_C$ it remains on the upper curve and at $\theta_H = \frac{\pi}{2} - \theta_C$ it moves on the lower curve. This situation is shown in Fig. 8. The dashed curve shows the equilibrium solutions that are corresponding to energy maxima and are unstable. If *h* is more than 1, then θ_R reaches $\frac{\pi}{2}$ when $\theta_H = \frac{\pi}{2}$.

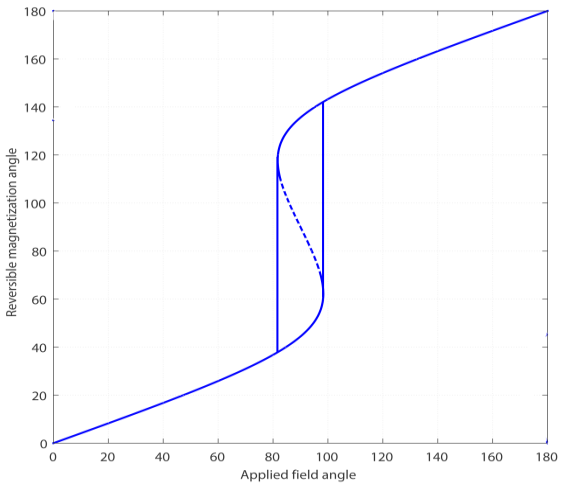

Fig. 7. Reversible magnetization angle (θ_R) vs applied field angle (θ_H) in rotation mode (*h*=0.7).

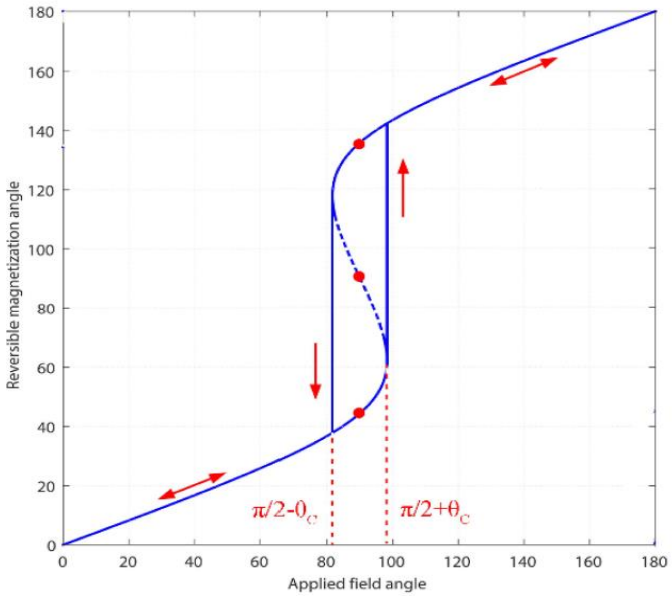

Fig .8. Hysteresis behavior of Reversible magnetization angle

In both modes of M_R rotation, if θ_{R0} is the magnetization angle corresponding to θ_{H0}, then $\pi - \theta_{R_0}$ is the magnetization angle corresponding to $\pi - \theta_{H_0}$. In other words, when plotting on the interval [0,π], the point $(\theta_H, \theta_R)=(\frac{\pi}{2},\frac{\pi}{2})$ is the center of odd symmetry as shown in Fig. 9.

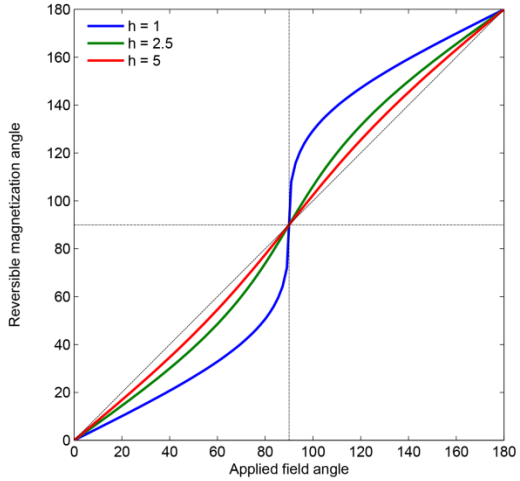

Fig.9. Reversible magnetization angle (θ_R) vs applied field angle (θ_H) for h >1.

3.7 Bifuraction Curve

We can decompose the normalized applied field, *h*, into parallel and perpendicular components to the easy axis by defining: $h_x = h * \cos(\theta_H)$ and $h_y = h * \sin(\theta_H)$. Therefore, Eq.1 becomes:

$$\sin\theta_R \cos\theta_R + h_x \sin\theta_R - h_y cos\theta_R = 0 \qquad (6)$$

In terms of number of equilibrium states and energy minima, in a specific applied field, there exists a curve C on the $h_x - h_y$ plane such that when the applied field is inside the curve, Eq. 6 has three equilibrium states (either two energy minima and one energy maxima or one energy minima and two energy maxima). When the applied field is outside the curve, Eq. 6 has one equilibrium state that is energy minima. To derive the equation of C, using the method of bifurcation curve, and by applying:

$$\frac{\partial}{\partial\theta_R}\{\sin\theta_R \cos\theta_R + h_x \sin\theta_R - h_y cos\theta_R\} = 0, \qquad (7)$$

the following asteroid equation is obtained:

$$h_x^{\frac{3}{2}} + h_y^{\frac{3}{2}} = 1 \qquad (8)$$

In Fig.10, for $h<0.5$, the applied field vector remains inside the asteroid for any applied field angle and oscillation occurs. For $h>1$, the applied field vector will be outside the asteroid for any applied field angle and rotation occurs. For the values of $0.5<h<1$, a circle with radius of *h*, intersects the asteroid. This results in the behavior of reversible magnetization angle introduced in Fig. 8. To find the switching applied field angles of $\frac{\pi}{2} + \theta_C$ and $\frac{\pi}{2} - \theta_C$, note that the parametric equation of the asteroid is $(h_x, h_y) = (\cos^3\theta_H, \sin^3\theta_H)$. Therefore, θ_C is given by:

$$\cos^6 \theta_C + \sin^6 \theta_C = h^2 \quad (8)$$

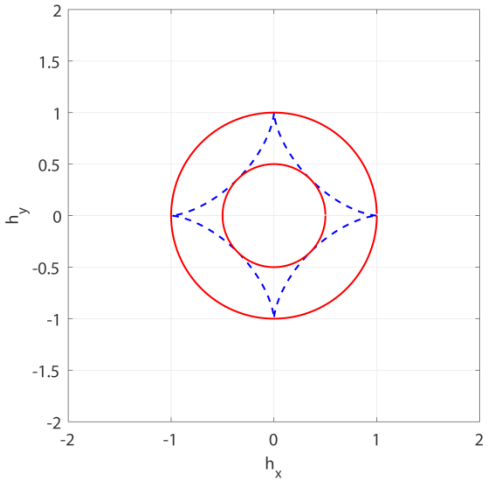

Fig. 10. Bifurcation curve together with two circles of *h*=0.5 and *h*=1

3.8 Simulation and Experimental Results

Applying the model algorithm, the total magnetization, *M*, is computed as the vector sum of reversible and irreversible components. Figure 11 shows the model results: the angle of total magnetization, θ_M, plotted against applied field angle, θ_H, for different values of *h* normalized to the coercive field, H_C.

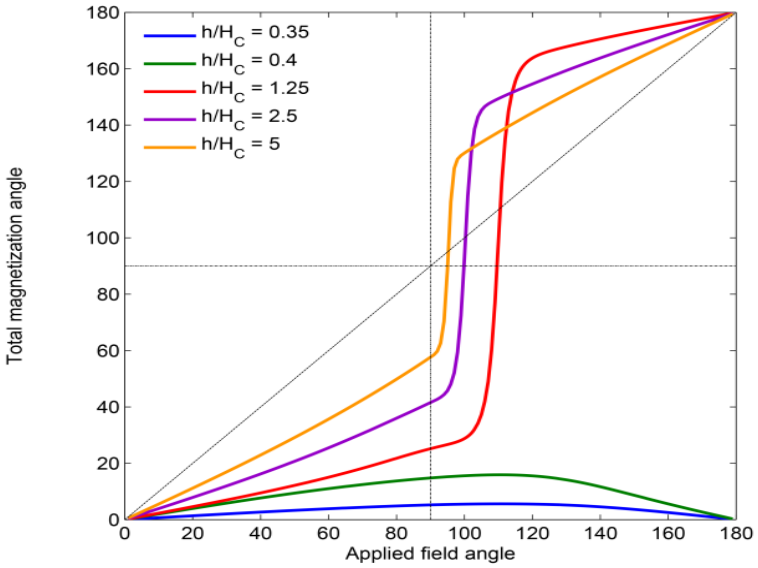

Fig. 11. Total magnetization angle (θ_M) vs applied field angle (θ_H).

Measurements were obtained using a sample of magnetic tape (diameter of 5 mm and height of 1 mm) and a vibrating sample magnetometer (VSM). The scalar measurements along the easy axis showed coercivity of 675 G and squareness of 0.7. Setting X-axis and Y-axis to be along easy and hard axis of the sample, respectively, a negative saturation field of -10000 G is applied and increased to the fixed positive value, H. The field is then rotated clockwise with increments of 10^0 to complete 360^0 of rotation while X- and Y-components of magnetization are being recorded. The magnetization angle θ_M is calculated using the two magnetization components.

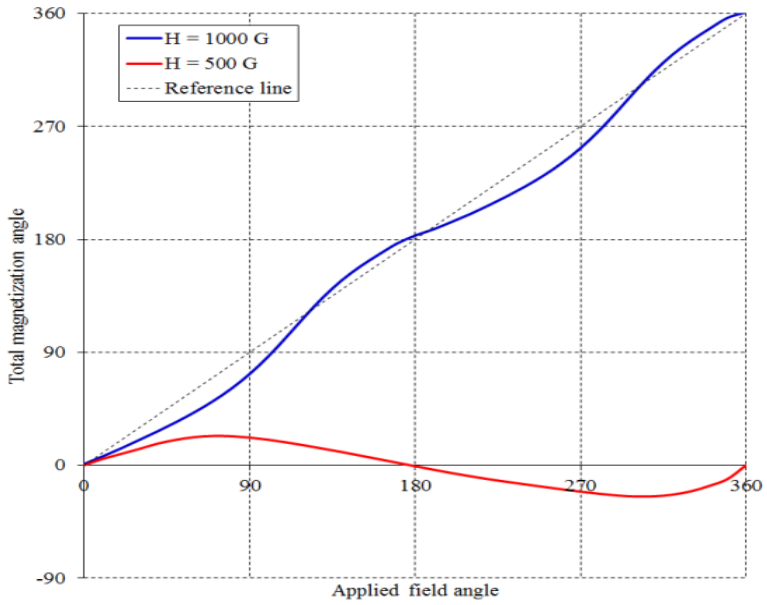

Fig.12. Measurment of total magnetization angle (θ_M) vs applied field angle (θ_H) for a sample of magnetic tape showing oscillation and rotation modes.

The results for two different applied fields of 1000 G (rotation) and 500 G (oscillation) are shown in Fig. 12. In oscillation mode, as the field decreases, the range of oscillation decreases. In rotation mode, as the field increases, the curve tends to approach the reference line. For values of applied fields close to the coercivity, since the irreversible component is very small, noise distorts the measurement significantly.

3.9 Conclusion

The proposed model decomposes the magnetization into reversible and irreversible components to model the total vector magnetization of a distribution of uniaxial particles. The irreversible magnetization and the magnitude of the reversible magnetization are modeled through previous studies by the authors and were not repeated to avoid

redundancy. The main objective of this chapter is: 1) to account for the irreversible magnetization as a unique process and 2) to use an SW approach to model the angle of the reversible magnetization. The model results show the same behavior observed in the measurements. The model reduces to the classical SW model at small and large fields. The current version of the model is only applicable to a distribution of single-domain particles. The additional complication of domain wall motion requires nontrivial changes to use the model with multidomain particles.

Chapter 4: A Vector Model for Off-Axis Hysteresis Loops Using Anisotropy Field

4.1 background

The Stoner-Wohlfarth (SW) model is widely used to model the magnetization of a single domain ellipsoid particle as a function of an external magnetic that was discussed in chapter 3. A general review of various magnetic modeling techniques is given in [DEL,2015]. Another review focused on modeling rotational magnetization for energy loss calculations is given in Ref. 3. Recent work modified the SW model to simulate anisotropic media by including different distributions for particles orientations with tunable parameters representing different anisotropic dispersions [DEL,2000], [STA,1997].

The anisotropy field (AF) model of vector magnetization is presented for a distribution of uniaxial particles as a generalization of the Stoner-Wohlfarth model. The magnetization is uniquely decomposed and is computed as the sum of an irreversible component, $\mathbf{M_I}$, and a reversible component, $\mathbf{M_R}$ [DEL,2006]. The model assumes that $\mathbf{M_I}$ is a function only of the applied field and defines the magnetic state of the particle. The magnetic state of the system is the contribution to $\mathbf{M_I}$ as a function of the critical field of the particle which depends on the orientation of the applied field. The locus of points of the critical field is a function of the direction of orientation of the applied field. This locus is a closed surface called the critical surface. For a uniaxial particle, the critical surface could be an ellipse with the easy axis along its minor axis. As long as the applied field lies inside the critical surface, $\mathbf{M_I}$ is unchanged. Upon exiting the critical surface, $\mathbf{M_I}$ will

switch to align with the nearest easy axis. On the other hand, $\mathbf{M_R}$ is a function of the magnetic state as well as the applied field. The direction of $\mathbf{M_R}$ is determined by minimizing the sum of the magnetocrystalline uniaxial anisotropy energy and the Zeeman energy.

In this chapter, we used a different approach to derive the direction of reversible component to account for anisotropy by incorporating a vector realization of an equivalent anisotropy field ($\mathbf{H_k}$). The absolute value of this field is given by αM_S, where α is an appropriate constant and M_S is the value of the saturation magnetization. Then, the vector $\mathbf{M_R}$ will point in the direction of the net field, which is the vector sum of $\mathbf{H}$ and $\mathbf{H_k}$ as shown in Fig. 13.

Similar to the model introduced in [DEL,2015], the total magnetization, $\mathbf{M}$, is the vector sum of the irreversible magnetization, $\mathbf{M_I}$, and the reversible magnetization, $\mathbf{M_R}$. In order to uniquely determine the magnetization, we need to express the magnitudes and the directions of these two components. The magnitude of $\mathbf{M_I}$ is computed by a scalar Preisach differential equation approach [VAJ,1993] and the direction of $\mathbf{M_I}$ is along the easy axis. The magnitude of $\mathbf{M_R}$ is computed by a magnetization-dependent function [DEL,2000] and its direction is along the vector sum of the applied field and the anisotropy field.

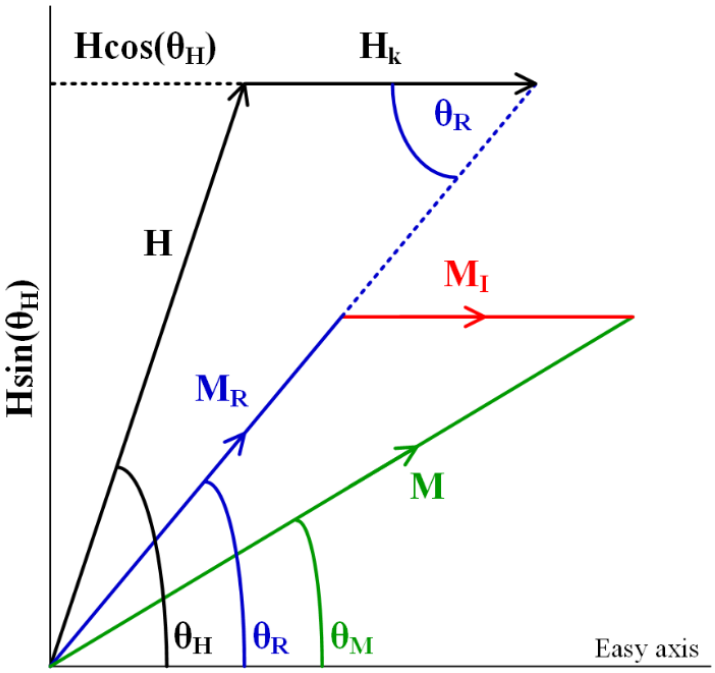

Fig. 13. Graphical realization of the model. Graphical realization of the model. All angles are measured from the easy axis. M_I is the irreversible magnetization, M_R and θ_R are the reversible magnetization and its angle, M and θ_M are the total magnetization and its angle, and H and θ_H are the applied field and its angle. H_k is the anisotropy field.

4.2 overview

A model for the off-axis vector magnetization of a distribution of uniaxial particles is presented. Recent work by the authors decomposed the magnetization into two components and modeled the total vector magnetization as their vector sum. In this chapter, to account for anisotropy, the direction of the reversible magnetization component is specified by the vector sum of the applied field and an effective anisotropy field. The formulation of the new anisotropy field (AF) model is derived and its results are discussed considering (i) oscillation and rotational modes, (ii) lag angle, and (iii) unitary magnetization. The

advantages of the AF model are outlined by comparing its results to the results of the classical Stoner-Wohlfarth model.

4.3 **Gibb's Free Energy Function**

To derive the Gibb's energy function for the anisotropy field (AF) model, we start by the trigonometric relationship illustrated in Fig. 13, hence:

$$tan(\theta_R) = \frac{Hsin(\theta_H)}{H_k + Hcos(\theta_H)} \quad (9)$$

which can be simplified to:

$$H_k sin(\theta_R) + Hcos(\theta_H)\, sin(\theta_R) = Hsin(\theta_H)\, cos(\theta_R) \quad (10)$$

or:

$$Hsin(\theta_H - \theta_R) = H_k sin(\theta_R) \quad (11)$$

By defining the anisotropy field, $H_k = \frac{K_U}{M_R}$, where K_U is the uniaxial magnetocrystalline anisotropy constant, and M_R is the saturation magnetization, we obtain:

$$M_R Hsin(\theta_H - \theta_R) - K_U sin(\theta_R) = 0 \quad (12)$$

By integration with respect to θ_R, the Gibb's Energy function that corresponds to equation (12) is:

$$W = -M_R H\, cos(\theta_H - \theta_R) - K_U cos\theta_R \quad (13)$$

while the energy function for a uniaxial particle according to the Stoner-Wohlfarth model is:

$$W = -M_R H\, cos(\theta_H - \theta_R) - K_U cos^2\theta_R \quad (14)$$

It's noted that the Zeeman component of the energy that gives the interaction between the applied field and the particle's magnetic moment is the same for both the AF and SW models. The magnetocrystalline uniaxial anisotropy component of the energy is $K_U \cos\theta_R$ in the AF model rather than $K_U \cos^2\theta_R$ in the SW model. This removes the limitations of the SW model that is the crossover of the hysteresis branches before the switching field when the applied field angle is close to 90 degrees.

4.4 **Oscillation and Rotational Modes**

Following the same analytical procedure in [DEL,2016], and defining the normalized applied field as $h = \frac{HM_R}{2K_U}$, Eq. 12 becomes:

$$2h \times sin(\theta_H - \theta_R) - sin(\theta_R) = 0 \quad (15)$$

The magnetization oscillation mode occurs when a sufficiently small rotational applied field results in a magnetization that does not rotate with the field. Instead, it just oscillates around the easy axis. In [DEL,2016] we showed that in the SW model, the oscillation occurs when *h* is less than 0.5. In this section, we will prove mathematically that this threshold is also valid for the AF model. Equation 15, states the reversible magnetization angle θ_R as an implicit function of the applied field angle θ_H. Oscillation occurs if this function has a maximum point.

Equation 7 can be rewritten as:

$$sin\theta_H \, cot\theta_R - cos\theta_H = \frac{1}{2h} \quad (16)$$

By taking implicit derivative with respect to θ_H:

$$\frac{d\theta_R}{d\theta_H} = \frac{cos\theta_H \, cot\theta_R + sin\theta_H}{sin\theta_H \, csc^2 \, \theta_R} = 0 \quad (17)$$

$$cot\theta_R = -tan\theta_H \quad (18)$$

$$\theta_R + \frac{\pi}{2} = \theta_H \quad (19)$$

The result obtained through Eq. 19 proves that the AF model has the same locus for the maximum points as the SW model [DEL,2016]. By plugging Eq. 19 into Eq. 8:

$$sin(\theta_R + \frac{\pi}{2})\, cot\theta_R - cos(\theta_R + \frac{\pi}{2}) = \frac{1}{2h} \quad (20)$$

$$cos\theta_R cot\theta_R + sin\theta_R = \frac{1}{2h} \quad (21)$$

$$sin(\theta_R) = 2h \quad (22)$$

which shows that Eq. 15 has a maximum if h<0.5, as shown in Fig. 14.

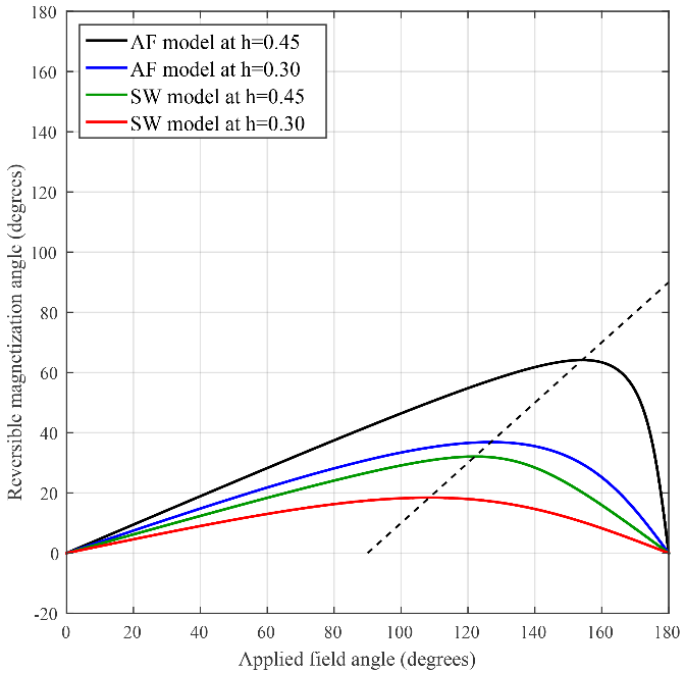

Fig. 14. Comparison between reversible magnetization angle (θ_R) versus applied field angle (θ_H) in the oscillation mode (h < 0.5) of the AF and SW models. Dashed line: locus of maximum θ_R for both models.

The magnetization rotational mode refers to the situation when the magnetization vector tends to follow the rotational applied field. In both the AF and SW models, rotation

occurs when h>0.5.

The SW model suggests an odd symmetry with respect to the point $(\frac{\pi}{2}, \frac{\pi}{2})$, as shown in Fig. 15a. This means that the lag angle has a period of π for the SW model. However, the period of the lag angle derived for the AF model is 2π, as shown in Fig. 15b, which is typical for several anisotropic media. In both models, as the applied field magnitude increases, the magnetization angle curves approach the reference line because for large applied fields the Zeeman energy is significantly larger than the magnetocrystalline uniaxial anisotropy energy and the magnetization aligns itself perfectly with the applied field.

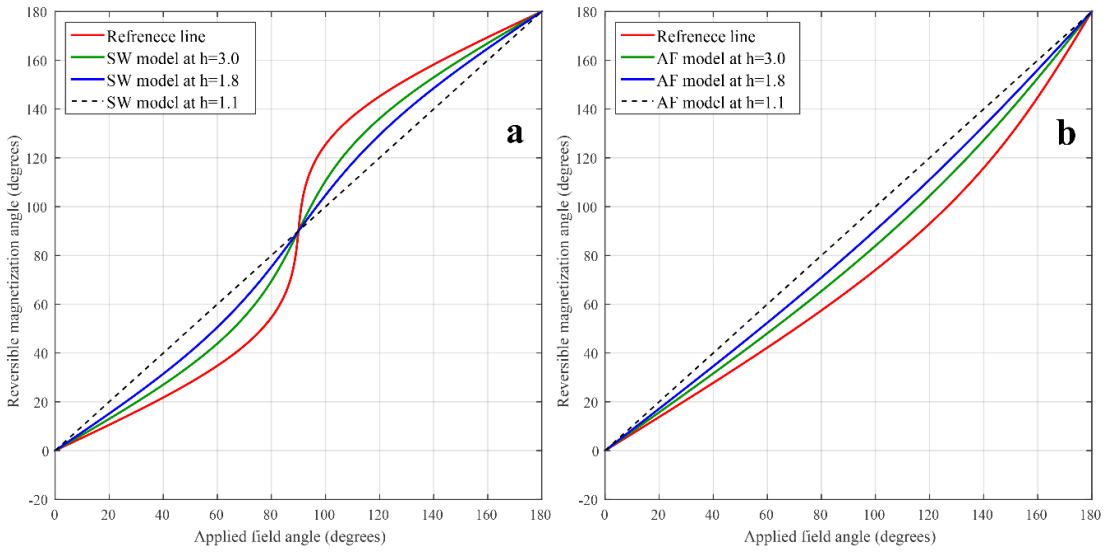

Fig. 15. Behavior of (a) the Stoner-Wohlfarth model and (b) the anisotropy field model in the rotational mode of magnetization.

4.5 Bifurcation Curve

Defining $h_x = h\cos(\theta_H)$ and $h_y = h\sin(\theta_H)$ to be the two components of normalized applied field, *h*, in the x and y directions, the Gibb's energy function for the AF model can be rewritten as:

$$W_{AF} = -h\cos(\theta_H - \theta_R) - \frac{1}{2}cos\theta_R = -h_x \cos\theta_R - h_y \sin\theta_R - \frac{1}{2}cos\theta_R \quad (23)$$

Similarly for the SW model:

$$W_{SW} = -h_x \cos\theta_R - h_y \sin\theta_R - \frac{1}{2}cos^2\theta_R \quad (24)$$

The equilibrium solution(s) refers to the value(s) of θ_R corresponding to $\frac{\partial W}{\partial \theta_R} = 0$. This solution could be either a minimum (stable equilibrium) or a maximum (unstable equilibrium). A bifurcation curve is a closed curve in the $h_x - h_y$ plane that specifies regions with different number of equilibrium solutions. To derive the equation of the bifurcation curve, we need to eliminate θ_R from the system of $\frac{\partial W}{\partial \theta_R} = 0$ and $\frac{\partial^2 W}{\partial \theta_R^2} = 0$ equations. For the AF model we have:

$$\frac{\partial W}{\partial \theta_R} = h_x \sin\theta_R - h_y \cos\theta_R + \frac{1}{2}\sin\theta_R = 0 \quad (25)$$

$$\frac{\partial^2 W}{\partial \theta_R^2} = h_x \cos\theta_R + h_y \sin\theta_R + \frac{1}{2}\cos\theta_R = 0 \quad (26)$$

Therefore:

$$(h_x \sin\theta_R - h_y \cos\theta_R)^2 + (h_x \cos\theta_R + h_y \sin\theta_R)^2 = \left(-\frac{1}{2}\sin\theta_R\right)^2 + \left(-\frac{1}{2}\cos\theta_R\right)^2 = \frac{1}{4} \quad (27)$$

so that:

$$h_x^2 + h_y^2 = \frac{1}{4} \quad (28)$$

This should be compared to the famous astroid equation of the SW model:

$$h_x^{\frac{2}{3}} + h_y^{\frac{2}{3}} = 1 \quad (29)$$

In the $h_x - h_y$ plane, a rotational applied field with a constant magnitude, h, would follow a circular path of radius h. If h<0.5, for both models, all the points on this path would fall inside the bifurcation curve and oscillation mode occurs. Also for both models, h>0.5 results in rotational mode, however, in the SW model, due to the complexity of the solution and the shape of the astroid, this range has to be divided into two sub intervals of 0.5<h<1 and h>1, as explained in detail in [DEL,2016], but for the AF model, this consideration is unnecessary.

4.6 **Unitary Magnetization**

The scalar unitary magnetization is the projection of the total magnetization vector along the applied field direction. Figure 4 show the unitary magnetization versus the normalized applied field at different applied field angles for both the AF and SW models. It's clear that the SW model shows a crossover of the hysteresis loop branches for an applied field angle of 85 degrees (Fig. 16a), while the AF model (Fig. 16b) does not. This SW model limitation is nonexistent in the AF model.

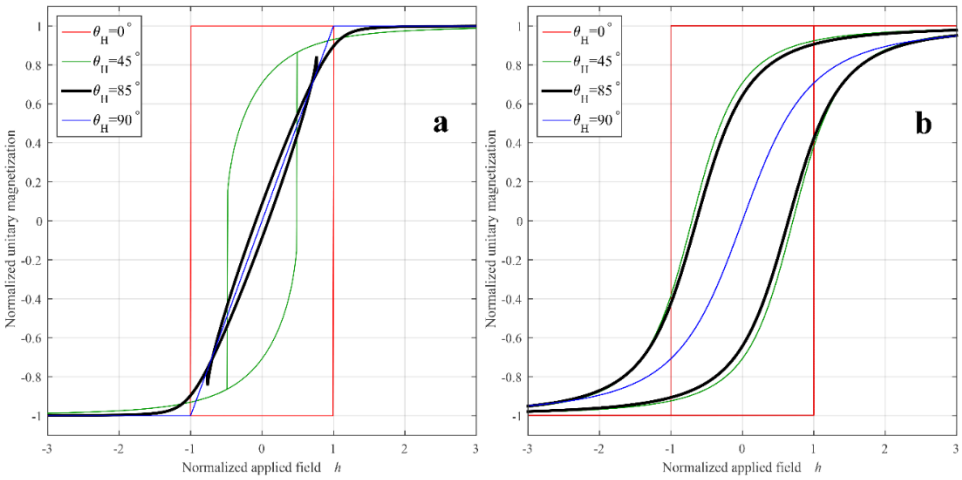

Fig. 16. Unitary magnetization for applied field angles of 0, 45, 85, and 90 degrees of (a) the Stoner-Wohlfarth model and (b) the anisotropy field model. The Stoner-Wohlfarth crossover limitation can be seen at the 85-degree applied field angle.

The SW model predicts a switching field for the unitary magnetization hysteresis loops, as demonstrated by the discontinuous jumps in Fig. 16a. This switching field is the intersection of a circle of radius h_s with the astroid $h_x^{\frac{2}{3}} + h_y^{\frac{2}{3}} = 1$:

$$(h_s cos\theta_H)^{\frac{2}{3}} + (h_s sin\theta_H)^{\frac{2}{3}} = 1 \quad (30)$$

$$h_s = (\cos^{\frac{2}{3}}\theta_H + \sin^{\frac{2}{3}}\theta_H)^{\frac{-3}{2}} \quad (31)$$

However, the unitary magnetization hysteresis loops of the AF model are continuous over the 1-<*h*<1 range, as seen in Fig. 16b, and a conventional switching field does not exist. This is a typical behavior of several anisotropic media. The hysteresis loops for both models have unit squareness at $\theta_H = 0$ and they are totally reversible at $\theta_H = 90$.

4.7 Conclusion

An off-axis vector magnetization model based on the decomposition of the magnetization into a reversible and an irreversible component is introduced as the anisotropy field (AF) model. In this model, the direction of the reversible component is specified by vector summation of the applied field and an equivalent anisotropy field. The graphical realization of the AF model is presented, followed by the mathematical derivation of its Gibb's free energy function. The behavior of the AF model in the oscillation and rotational modes of magnetization, its lag angle curves, its bifurcation curve equation, and its unitary magnetization curves at different applied field angles are discussed and compared to the Stoner-Wohlfarth (SW) model. The results show that the AF model is capable of simulating the vector magnetization behavior of anisotropic media, namely: (i) the lag angle plots of period 2π and the continuous unitary magnetization hysteresis loops. This was achieved by incorporating an irreversible magnetization component and accounting for the anisotropy

using an effective anisotropy field. The AF model (i) does not show a unitary magnetization cross over for applied field angles between 80 and 90 degrees, (ii) has a faster algorithm than the SW model due to the simplicity of its bifurcation curve, and (iii) is already generalized to a distribution of uniaxial particles without the need for statistical distributions.

Chapter 5: Vector magnetization of a distribution of cubic particles

5.1 Background

Modifications and extensions of the Stoner-Wohlfarth model have been widely used to model vector magnetization in different anisotropic dispersions [KUN,2015]. In chapters 3 and 4, I introduced the vector model for the magnetization of distribution of uniaxial particles. This model combines the classical Stoner-Wohlfarth model [STO,1991] with the idea of decomposing magnetization into unique reversible and irreversible components with a simple method for identifying the parameters of each process. In this chapter, we generalized the idea to cubic anisotropy projected to (100) plane that has easy axes of x-axis and y-axis and hard axes of y=x and y=-x in regular Cartesian coordinate system.

Similar to the model introduced in [DEL,2016], the total magnetization is the vector sum of the irreversible magnetization, M_{I}, and the reversible magnetization, M_R. In the case of uniaxial media, the direction of M_{I} is perpendicular to the single hard axis (i.e. parallel with easy axis) but in the case of cubic anisotropy projected to (100) plane, M_{I} has two components perpendicular to each of hard axes. The magnitude of each component of M_{I} is determined by differential equation approach [KAH,2004]. On the other hand, the magnitude of M_{R} is computed by a single-valued function of the applied field and its direction is determined by the modified Stoner-Wohlfarth model. Note that the susceptibility of M_{R} along the easy axis is zero and the total magnetization is parallel to an easy axis when a sufficiently large field is applied along it.

5.2 Overview

A model for the vector magnetization of single-domain particles is presented. In previous chapters, we modeled the vector magnetization of uniaxial particles. In this chapter, we generalized the idea to the cubic anisotropy projected to (100) plane with an energy approach applicable to a generic plane. The direction of anisotropy field is introduced based on the Stoner-Wohlfarth model resulting in the reversible component of the magnetization and then the irreversible components of the magnetization are added to generate the total magnetization vector. Comparisons with uniaxial particles are made to show the validity of this generalization.

5.3 Energy Approach

Stoner-Wohlfarth particles are single domain planar structures with uniaxial anisotropy, immersed in a uniform magnetic field $\boldsymbol{H_a}$. In this section, we describe the case of particles having different magnetic anisotropy.

Two components of the energy are the cubic anisotropy energy and the Zeeman energy. The 3D expansion of the cubic anisotropy energy density is:

$$W_C = K_1(\alpha^2\beta^2 + \alpha^2\gamma^2 + \beta^2\gamma^2) + K_2\alpha^2\beta^2\gamma^2 \quad (32)$$

Where α, β and γ are direction cosines with respect to x,y and z-axes. Define θ_R as the angle between M_R and the x-axis, and θ_H as the angle between the applied field and x-axis and applied field, h, that is normalized to the anisotropy field ($h = \frac{H}{H_K}$). We can derive a general expression for the normalized Gibb's free energy by evaluating the 3D anisotropy

energy density on a generic plane given by $z = ax + by$ that passes through the origin of the Cartesian system of reference; this assumption does not lead to a loss of generality, due to the cubic symmetry of the energy density.

Refer to equation (32) and with assumption that $K_1 \gg K_2$, in order to obtain the in-plane magnetic anisotropy we must evaluate the relationship between the three directional cosines α, β and γ. The straight line associated to the unitary magnetization vector, and passing through the origin is given in parametric form by: $x = \alpha t, y = \beta t, z = \gamma t$

Now we compute the orthogonal projection of this straight line on the plane.

$$\begin{cases} x = \alpha t \\ y = \beta t \\ z = \gamma t \\ z = ax + by \end{cases} \xrightarrow{yields} \begin{cases} x = \alpha t \\ y = \beta t \\ z = (a\alpha + b\beta)t \end{cases} ; \ \gamma = a\alpha + b\beta$$

(33)

Clearly, the obtained directional cosines are no longer normalized to 1; for this reason, we must scale these quantities in order to compute the new components of the unitary magnetization vector on the plane.

$$c \stackrel{\text{def}}{=} \alpha^2 + \beta^2 + \gamma^2 = (1 + a^2)\alpha^2 + (1 + b^2)\beta^2 + 2ab\alpha\beta; \quad (34)$$

$$\alpha' = \frac{\alpha}{\sqrt{c}}, \beta' = \frac{\beta}{\sqrt{c}}, \gamma' = \frac{\gamma}{\sqrt{c}} \quad (35)$$

Finally, by adding the Zeeman energy, we can write the normalized Gibb's free energy:

$$g_L = K_1(\alpha'^2\beta'^2 + \beta'^2\gamma'^2 + \gamma'^2\alpha'^2) - \alpha h_x - \beta h_y = \frac{K_1}{c^2}[a^2\alpha^2 + 2ab\alpha^3\beta + (1 + a^2 + b^2)\alpha^2\beta^2 + 2ab\alpha\beta^3 + b^2\beta^4] - \alpha h_x - \beta h_y \quad (36)$$

From this general expression it is possible to derive the special cases of interest. For example, if the plane is z=0 (xy plane), by setting γ=0 ($\alpha^2+\beta^2=1$), it is easy to show that the

classic biaxial anisotropy ((100) cubic anisotropy) is obtained:

$$g_L^{100} = \frac{1}{8}\sin^2 2\theta_R - h_x \cos\theta_R - h_y \sin\theta_R \quad (37)$$

By taking derivatives of (9) and using $h_x = h * cos(\theta_H)$ and $h_y = h * sin(\theta_H)$, we can verify the relationship between θ_R, θ_H and h for cubic anisotropy projected in (100) plane is:

$$\frac{1}{4}\sin(4\theta_R) - h\sin(\theta_H - \theta_R) = 0 \quad (38)$$

Also note that the corresponding relationship between θ_R, θ_H for uniaxial particles is introduced in [DEL,2016] as:

$$\frac{1}{2}\sin(2\theta_R) - h\sin(\theta_H - \theta_R) = 0 \quad (39)$$

5.4 Direction of The Anisotropy Field

Anisotropy field, H_k is an equivalent field with a magnitude of $H_k = \frac{2K_1}{M_S}$ (M_S is the saturation magnetization) that is used in most reference [PET,2011]. In [JAM,2016] we assumed that for uniaxial particles, anisotropy field remains parallel with easy axis and we derived a simple model that is comparable with SW model. In this section, we used equation (38) for cubic anisotropy projected to (100) plane and equation (39) for the uniaxial anisotropy to derive a direction for the anisotropy field consistent with the SW model.

For the case of uniaxial, equation (8) can be written as:

$$\frac{\frac{1}{2}H_k}{sin(\theta_H - \theta_R)} = \frac{H}{\sin(2\theta_R)} \quad (40)$$

Using the sine law, the graphical visualization shown in Fig.17 is consistent with this equation if we choose $a = 2$ and $c = \frac{1}{2}$.

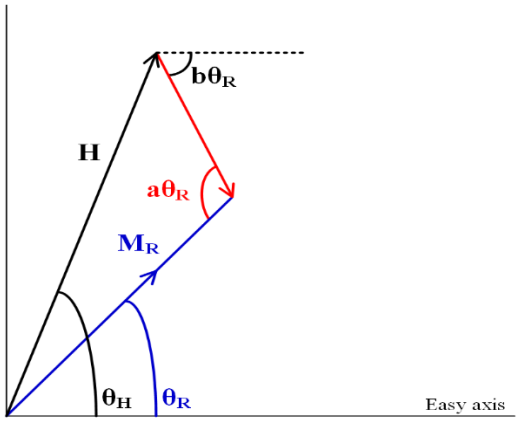

Fig.17. Visualization of the Stoner-Wohlfarth model: for the classical SW (a,b,c)=(2,1,0.5) and for the modified SW model with cubic anisotropy projected to (100) plane (a,b,c)=(4,3,0.25)

By applying basic geometry, $a\theta_R = b\theta_R + \theta_R$, gives $b = a - 1 = 1$ stating that the angle that the anisotropy field, H_k makes with the x-axis is $-\theta_R$, that is when M_R rotates counterclockwise the anisotropy field rotates clockwise with the same angular frequency. M_R and anisotropy field lie in the same direction only when they are along the easy axis and are in opposite direction when they are along the hard axis (in this case y-axis). Note that as M_R rotates 90^o, the anisotropy field also rotates -90^0 and will be located in the opposite direction of M_R.

For the case of cubic anisotropy projected to (100) plane, equation (38) can be written as:

$$\frac{\frac{1}{4}H_k}{sin(\theta_H - \theta_R)} = \frac{H}{\sin(4\theta_R)} \tag{41}$$

That is consistent with Fig.1 using $a = 4$, $b = a - 1 = 3$ and $c = 0.25$

Now the angle between the anisotropy field and the x-axis is $-3\theta_R$. Again, by inspection, we can verify that the anisotropy field and M_R are in the same direction only along easy axis and they are in the opposite direction along hard axis. For example, noting that $y = x$ is a hard axis, as M_R rotates 45^o, the anisotropy field rotates -135^o and is placed in the opposite direction of M_R.

The method is similar to the image theory in electromagnetics and shows that anisotropy field plays a significant role in analyzing and modeling of vector magnetization. It can be extended for biaxial anisotropy with non-perpendicular easy axes. Also, it can be generalized in 3D.

5.5 Simulation and Experimental Results

A. Total magnetization vector

A lot was said about reversible component of the magnetization and now we need to add the irreversible component to derive the total magnetization vector, *M*. In the case of uniaxial particles, we proposed that the irreversible component is along easy axis and its magnitude is computed by a Preisach differential-equation approach. In the case of cubic anisotropy, the irreversible component can be composed into two components, M_{Ix} and M_{Iy}, each perpendicular to the hard axes (that are y=x and y=-x). Note that this is consistent with the uniaxial case because in that case being along easy axis is equivalent to being perpendicular to the hard axis. The total magnetization is shown in Fig.18.

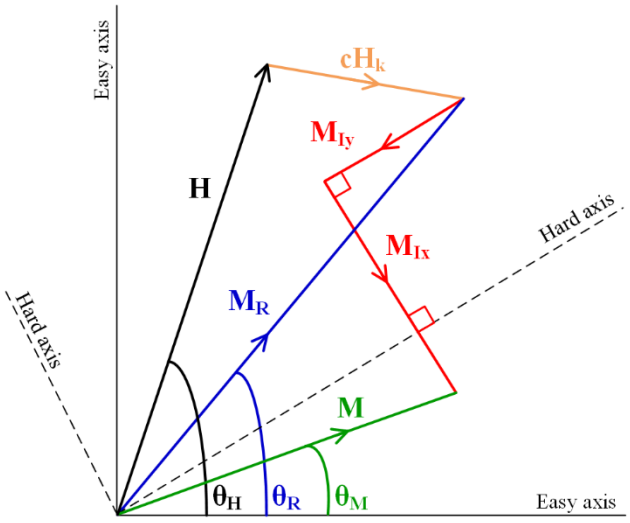

Fig.18. Graphical realization of the total magnetization for cubic anisotropy field.

B. Lag Angle Curves

Having magnitude and direction of irreversible and reversible components, the total magnetization can be uniquely determined. Lag angle is defined as the difference between applied field angle and magnetization angle. A computer simulation is performed based on assumptions of this model and the result for lag angle is shown in figure 19. As the field increases, the maximum lag angle decreases. Also, the applied field angle that this maximum occurs approaches 45 degrees (i.e. hard axis) as the field increases. The lag angle curve has a period of 180 degrees for uniaxial particles and a period of 90 degrees for cubic particles. The lag angle curve has a period of 180 degrees for uniaxial particles and a period of 90 degrees for cubic particles.

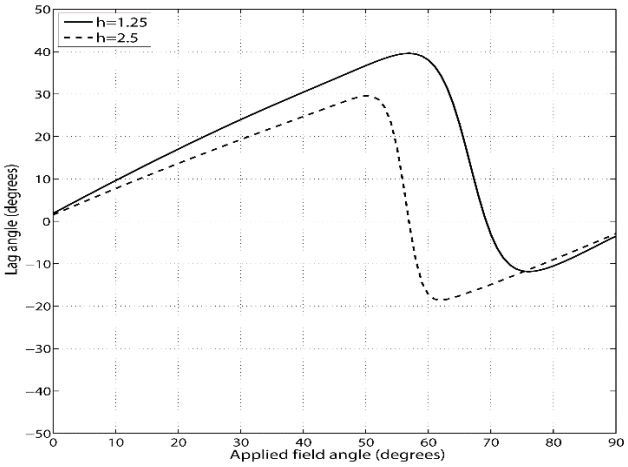

Fig.19. Lag angle curves for two different applied field magnitudes in rotation mode.

C. Magnetization Trajectories

Magnetization trajectory traced for a normalized applied field of h=1.25 is plotted in figure 20. Maximum magnitudes of magnetization occur along easy axes and minimum magnitudes are along hard axes. Note that the trajectory for uniaxial particles is elliptical with major axis along the single easy axis .

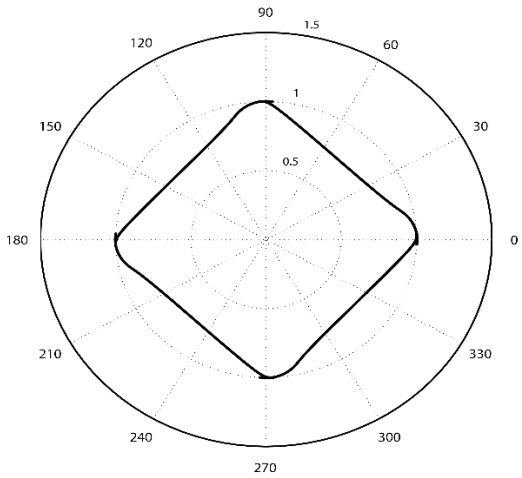

Fig.20. Cubic particle's magnetization trajectory for 360^{o} rotating applied field of normalized magnitude h=1.25 with magnetization normalized to its maximum value

D. Rotation, Oscillation and Bifurcation curve

Similar to the case of uniaxial particles, if the applied field is smaller than a threshold, then as the field rotates the magnetization will oscillate around the easy axis (oscillation mode). This threshold was shown to be *h*=0.5 since the bifurcation curve is an astroid. For cubic particles, the bifurcation curve is a *wind rose* and the rotation-oscillation threshold is *h*=0.25.

Considering that the parametric equation of the wind rose is

$$(h_x, h_y) = (5\cos^3 t - 6\cos^5 t\,, 5\sin^3 t - 6\sin^5 t) \tag{42}$$

The threshold can be derived by minimizing

$$h = \sqrt{(5\cos^3 t - 6\cos^5 t)^2 + (5\sin^3 t - 6\sin^5 t)^2} \tag{43}$$

For the values of $h < 0.25$, the applied field remains inside the bifurcation curve and does not change its state which refers to the oscillation mode.

5.6 Conclusion

A generalization of the model that was previously developed for uniaxial particles was developed in this work to model cubic anisotropy cut in (100) plane. A more general Gibbs free energy function were derived for projection of cubic anisotropy into any plane passing through origin. We showed that reversible component of magnetization can be derived using the Stoner-Wohlfarth model and we introduced a direction for the anisotropy field

consistent with Stoner-Wohlfarth model. The total magnetization is derived by adding two irreversible components to the reversible component. In terms of lag angle, the results show that the behavior of the total magnetization for cubic particle cut in (100) plane has a period of 90 degrees (half of the period of uniaxial particles) that is meaningful due to having two in-plane easy axes. More comparisons between two models were also made to ensure that the generalization is valid.

Chapter 6: Properties of Uniaxial Media Model

6.1 Background

Media consisting of aligned uniaxial particles have long been used for magnetic recording. Their unidimensional magnetic behavior along the easy axis has been accurately described by Preisach modeling. This chapter describes a three-dimensional model based on physical principles that extends the unidimensional models.

In previous chapters, I introduced a model for an ideal uniaxial media consisting of hysterons whose easy axes, EAs, are all parallel to the medium's EA [DEL,2016]. The model computes an irreversible magnetization component which lies along the EA that is sensitive to only the EA component of the applied field. An applied field rotates the magnetization to the minimum energy position. The reversible magnetization is the vector difference between the rotated magnetization and the irreversible magnetization. The anisotropy of the medium was introduced by an anisotropy field which limited the usefulness to small angles [JAM,2016]. We now use uniaxial anisotropy energy as the anisotropy source to lift this limitation. This technique was also used to describe media with cubic anisotropy [JAM,2017]. The result is that the remanence magnetization will always lie along the EA. Furthermore, if all the critical fields that switch a hysteron to a positive state are positive, the squareness of the major loop will be unity.

The irreversible magnetization component plays the role of the *state* of the system. It is computed as a function of the applied field only, and always points along the EA. In a rotating field, the magnetization changes by rotating to the new direction that minimizes

the energy, as well as changing its magnitude as the irreversible component changes. To get the reversible component, one simply subtracts the irreversible component from the magnetization. An advantage of this model as compared to classical model is that the state of the system can be measured at any time by simply reducing the applied field to zero. While in the classical model, it can only be computed, so that if errors accumulate when computing the state, it is not possible to correct it by direct measurement. The model has two characteristic modes in a rotating field: the oscillation mode and the rotation mode.

6.2 Model behavior

In the rotation mode, as the field starts to rotate, the magnetization will lag the applied field. In large fields, and for larger field angles, eventually, the irreversible magnetization will change sign. Since the direction of the magnetization must lies between the direction of the applied field and the nearest EA, the magnetization will now lead the applied field. Figure 21 illustrates this effect. The magnetization will change sign when the EA component, $H\cos\theta$, exceeds the coercivity, H_c, where H is the applied field. The variation of the crossing angle where the magnetization goes from lag to lead is illustrated in Fig. 22. The crossing angle, occurs when the applied field is equal to H_c and the critical angle is $\pi/2$. As the field is increased beyond H_c the critical angle increases to the maximum of π.

It is assumed that the medium consists of many particles that are tightly oriented towards the EA. Let φ be the average angle that the particles make with respect to the EA. A strong field along the EA will rotate particles towards the EA. When the field is reduced to zero, the particle magnetization will rotate back, and the measured squareness of the hysteresis loop will be cosφ. For a well aligned medium, the squareness is near unity. If we assume that the distribution of critical fields is Gaussian, then irreversible magnetization curves will be error functions as shown in Fig. 21. Thus, the ascending curve of a hysteresis loop is given by

$$M_I = M_S \mathrm{erf}\left(\frac{H_A - H_c}{\sigma}\right), \tag{44}$$

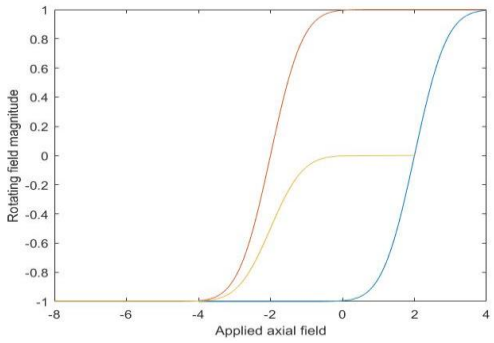

Fig. 21: Errorfunction approximation of the major loop and first order reversal curve.

The anisotropy energy is given by $W_a = K_u \sin^2\varphi$, where K_u is the anisotropy constant. Thus, the energy is a minimum when the magnetization is parallel to the EA. In a previous chapter, we had a similar model but there the anisotropy was described by an anisotropy field and the remanence of the particles was unique. To get the proper variation, one would have to change the field as the state of the system changes. Thus, the energy of a hysteron under the influence of both the anisotropy and an applied field, *H*, due to an applied field at angle θ *is* given by:

$$W = H_A M[\cos(\theta - \varphi)] + K_u \sin^2\varphi \, . \tag{45}$$

where H_A is the applied field, H_c is the coercivity, and σ is the standard deviation of the switching field. Then equilibrium is reached when W is a minimum as φ rotates. This is computed by setting the derivative of Eq. (45) equal to zero.

$$\frac{\partial W}{\partial \varphi} = H_A M_I[\sin(\theta - \varphi)] + 2K_u \sin\varphi \cos\varphi = 0. \tag{46}$$

It can be shown that the resulting point is a minimum by taking second derivatives.

Solving for θ, we get

$$\theta = \varphi - sin^{-1}\left[\frac{1}{k}\sin 2\varphi\right], \tag{47}$$

where $k = H_A M_I / K_u$. This equation can be used to compute the necessary applied field angle to achieve a certain direction of the magnetization. However, in the region where the EA component of the applied field is large enough to exceed the coercivity, then the irreversible magnetization will reverse, and hence, k will change sign.

It is noted that the argument of the arc sin must be less than one, therefore, k must be greater than one to have real solutions for all φ. Thus, the condition $k = 1$ is the critical field to go from oscillating mode to rotation mode. Hence the peak value for φ in the oscillating mode is half the arc sine of φ.

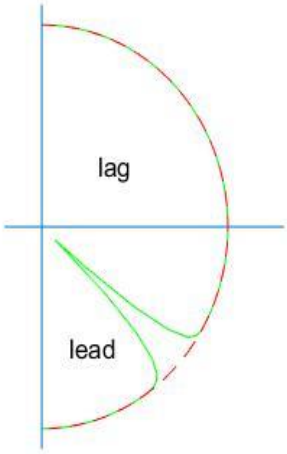

Fig.22: Magnetization (solid), applied field (dashed)

Upon rotation, as the EA component of the applied field approaches the coercivity of the medium, the irreversible magnetization begins to reverse, and the magnetization will start to spiral in towards the origin as shown in Fig. 22. The larger the applied field, the sooner it will begin to reverse. These magnetization reversal loci are useful in validating this model. The hangle-mangle curve will cross the zero lag-angle line at the point that the axial field component reaches the coercivity. From that point on, the magnetization leads the applied field. For a larger field, the curves will cross earlier, as shown in Fig. 23, where the angles are normalized to the angle at the coercivity.

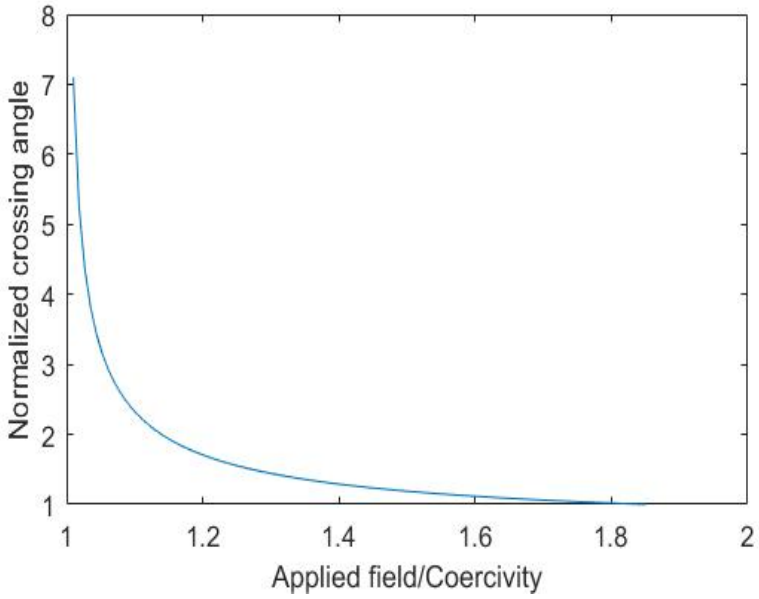

Fig. 23. Location of position of change from lag to lead,

Plotting the vector magnetization due to a rotating field is complicated due to hysteresis. Thus, in addition to following the change in magnetization, one must know the initial conditions. The state of the system at any time can be found by reducing the field to zero. The width of the dip in magnetization is determined by the steepness of the sides of the major loop. For example, if the sides of the major loop are vertical the width of the dip will be zero.

6.3 Hangle-mangle curves

The hangle-mangle curves describe the lag of the magnetization to the applied rotating field. These curves for uniaxial materials have a periodicity of π. They are also directly affected by the nature of the anisotropy. Since we have computed the applied field angle necessary to obtain a certain magnetization angle, there should not normally require

and additional work to plot one against the other. However, the calculation points for these variables do not line up.

For the anisotropy variation of in equation (47), Fig. 24 is the computed plot of the hangle-mangle curves. The problem is that in. equation (47), k is a function of Θ. So, there is no simple solution to the problem. We chose to approximate θ by φ in computing k

$$k = k_A \arccos\left[\operatorname{erf}\left(\frac{H_A \cos\varphi - H_c}{\sigma}\right)\right], \tag{48}$$

where k_A is the value of k (47), Using the same parameters used in Fig. 22, one gets the hangle-mangle shown in Fig. 24.

6.4 Standard tests

To check the validity of model, one must compare the model's behavior with standard tests. There are two types of tests that we have used: EA measurements, EAMs, including hysteresis loops and first order reversal curves, and spatial measurements, SMs, such as the vector magnetization due to a rotating field and hangle-mangle curves. The EAMs test for the applicability of the model to fit the data. The squareness should be very close to unity for the model to be applicable. Fitting the major loop is then used to determine the mean and the standard deviation of the critical field.

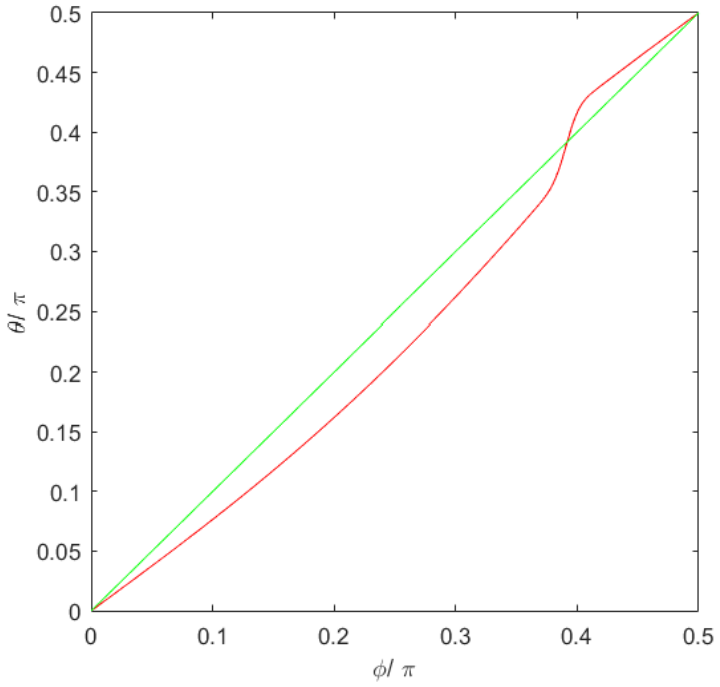

Fig. 24. Hangle-mangle curves for parameters in Fig. 23.

The SMs define the two regions of operation for the medium: the oscillation region and the rotation region. The magnetization trajectory starting from the easy axis for the first 90 of rotation traces out the arc of a circle. If the specimen is initially magnetized, hysterons with switching field larger in magnitude than the rotating field will not switch, so one must add their constant magnetization to the calculation. This will have the effect of shifting the loop. This has the effect of changing the apparent value of the coercivity. On the other hand, if we shift the center from the origin, we will get asymmetrical loops. These effects can be compared with experiment.

The most important consideration is the distribution of the vector moments of the hysterons. This will not only reduce the squareness to the mean of the cos θ, but also

decrease the depth of the dip in rotational magnetization. Both the standard deviations of the critical fields, σ, and the distribution of hysteron moments will affect the susceptibility at the sides of the hysteresis loops.

Prior to start the rotation of the magnetization the medium can be in several states. The hysterons with critical fields larger or smaller than extrema of the vertical field, the magnetization will not change. This has the effect of shifting minor loops vertically. For media with finite susceptibility, the coercivity will change, which in turn change the angular position of the magnetization dip.

6.5 Averaging over orientation

Let us review the model introduced in chapter 3. In this model, magnetization is vector sum of the reversible and irreversible components. The irreversible magnetization that is parallel with easy axis and does not change in direction is modeled by scalar Preisach model and the reversible component changes by Stoner-Wohlfarth model [2].

As stated before, The model is developed for behavior of the perfectly aligned hysterons. In this section of chapter 6, we improved the model by using a distribution in the hysteron easy axes. The net magnetization then is the weighted vector sum of the individual magnetizations. The previous model had three major inconsistencies with experimental results discussed below.

A) Squareness

Unitary magnetizations curves can be plotted by keeping the direction of the applied filed constant and plotting the projection of the magnetization along the applied

field with respect to the applied field magnitude. The squareness is defined as the ratio of saturation remanence to saturation magnetization and it measures how square is the hysteresis loop. Let α and ϕ be the polar and azimuthal angles of the easy axis respectively and θ be a the angle between magnetization and easy axis, by considering $p(\alpha, \phi)$ as the probability density function the general expression to calculate unitary magnetization is

$$\overline{\cos(\theta + \alpha)} = \frac{\iint \sin(\alpha)\cos(\theta+\alpha)p(\alpha,\phi)d\alpha d\phi}{\iint \sin(\alpha)p(\alpha,\phi)d\alpha d\phi} \qquad (49)$$

As shown in Fig.25, by applying the method of averaging over orientation and using a uniform distribution for both α and ϕ, the squareness of the unitary magnetization curves will be decreased and it results in smoother and more realistic curves.

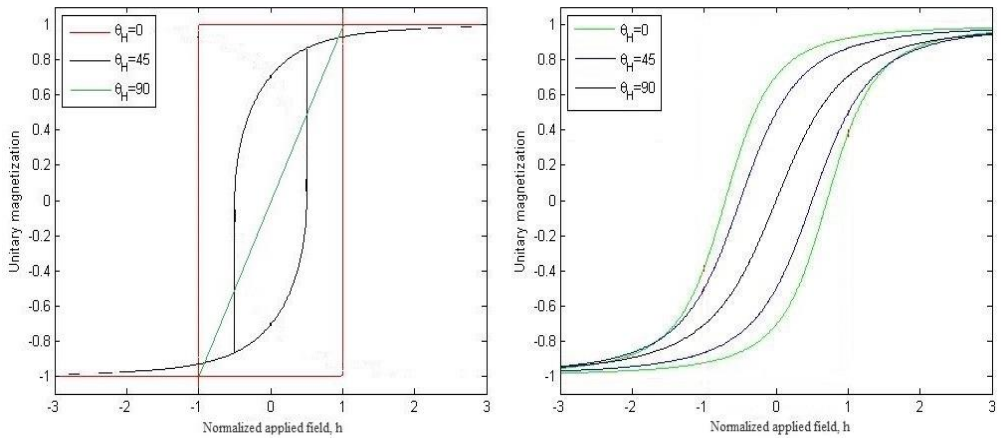

Fig.25. Unitary magnetization with (right) and without (left) averaging over orientation

B) The Jumps in Lag Angle

Lag angle curve is the magnetization angle versus applied field angle . We showed that for the normalized applied field, h, less than 0.5 the magnetization is not strong enough

to follow the applied field and oscillation mode will occur and rotation mode is for the values h more than 0.5 [DEL,2016]. Also we showed that there is a need to break down this range to 0.5<h<1 and h>1. In the previous model, for the normalized applied field in the range of 0.5 <h<1, we calculated jumps in lag angle. These jumps are not experimentally validated. The mathematical source of the jumps is the multiple intersections of a circle of radius h with the astroid representing the bifurcation curve of the uniaxial anisotropy [DEL,2016]. If we rotate the hysteron easy axes (equivalent with rotation of the astroid) then different intersections will be derived. Fig.26 shows how the discontinuity of the lag angle curves can be diminished by using a uniform distribution for α and ϕ.

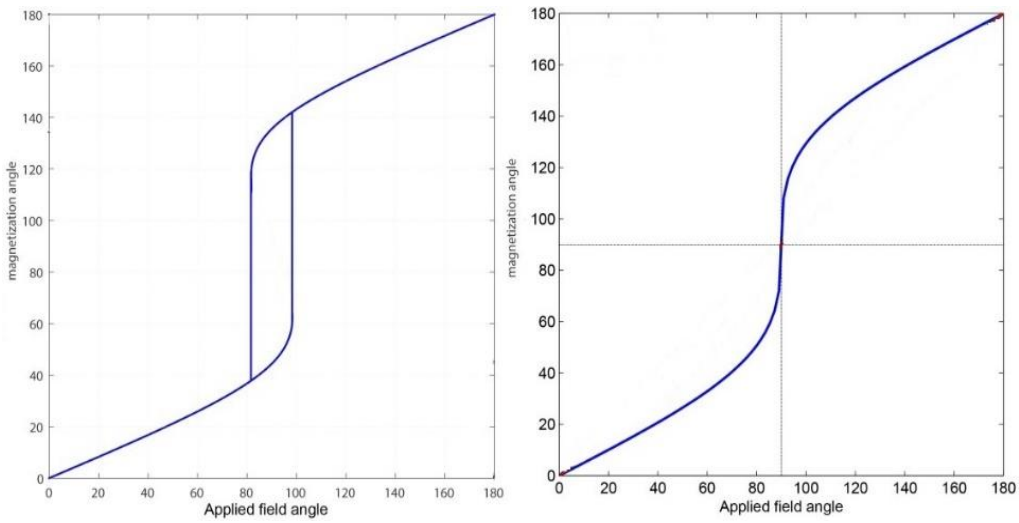

Fig.26. Lag angle curve with (right) and without (left) averaging over orientation

C) Magnetization at the Critical Angle

For the values of h>1, the previous model correctly predicted the lag angle magnetization behavior. The problem in this range is the small magnitude of magnetization at the critical

angle, that is where the magnetization changes from lagging to leading. At this angle, the magnetization vector is parallel with the applied field. This magnitude can be written as a function of the standard deviation of $p(\alpha, \phi)$.

6.6 Conclusions

The model presented discusses the two modes of the magnetization in a rotating field: the oscillation and rotation modes. In the rotation mode, for small fields the magnetization lags, but for fields greater than the coercivity, the magnetization leads the applied field. The model requires only a fit of the EA hysteresis loop by three parameters and the anisotropy constant to generate all the curves.

Chapter 7: Summery, Conclusion and Future Researches

In this dissertation, I developed a vector magnetization model for uniaxial media. In this model, magnetization is vector sum of reversible and irreversible components. The irreversible magnetization is modeled by scalar Preisach model and the reversible component changes by Stoner-Wohlfarth model. The model is developed for behavior of the perfectly aligned hysteron. A 3D model is presented for an assembly of hysterons as a generalization of the Stoner-Wohlfarth model. The magnetization is computed as the sum of an irreversible component, $\mathbf{M_I}$, and a reversible component, $\mathbf{M_R}$. This decomposition is unique. The model assumes that $\mathbf{M_I}$ is a function only of the applied field. The magnetic state of the system is the contribution to $\mathbf{M_I}$ as a function of the critical field of the hysteron. The critical field of the hysteron depends on the orientation of the applied field. The locus of points of the critical field is a function of the direction of orientation of the applied field. This locus is a closed surface called the critical surface. For a uniaxial hysteron, the critical surface could be an ellipse with the easy axis along its minor axis. As long as the applied field lies inside the critical surface, $\mathbf{M_I}$, is unchanged. Upon exiting the critical surface the irreversible magnetization will switch to alignment with the nearest easy axis.

On the other hand, $\mathbf{M_R}$ is a function of the magnetic state as well as the applied field. The direction of $\mathbf{M_R}$ is determined by minimizing sum of the magnetocrystalline uniaxial anisotropy energy and the Zeeman energy.

There is also a different approach to derive the direction of reversible component. This is done by considering anisotropy field. It is assumed that the anisotropy can be described by an equivalent field $\mathbf{H_k}$. This field is given by $\alpha\mathbf{M_S}$, where α is an appropriate

constant and $\mathbf{M_S}$ is the saturation magnetization. Then, the vector $\mathbf{M_R}$ will point in the direction of the net field, which is the vector sum of $\mathbf{H}$ and $\mathbf{H_k}$.

The idea is also generalized to create a model for the vector magnetization of a distribution of particles with cubic anisotropy. The model is extended to include cubic anisotropy projected to the (100) plane. The magnitude of the irreversible component is modeled using a Preisach differential-equation approach; however, other valid models can be used. The direction of the reversible component is modeled using the minimum energy approach of the classical Stoner–Wohlfarth model and taking into account the anisotropy field. The formulation of the generalized model is derived and its results are discussed considering oscillation and rotational modes, lag angle, and magnetization trajectories [JAM, 2017]

Averaging over orientation have been done to improve the model. By assuming that the distribution of critical fields is Gaussian, then the major loop will be an error function. For small rotating fields, the magnetization will oscillate between two extreme values on the same side of the origin. For larger fields, the irreversible magnetization can change sign and the magnetization will rotate about the origin. We start with a demagnetized specimen, then apply a field that starts along the easy axis and then rotates about the origin. For the first 90°, the magnetization will follow a circular path. Beyond that point the irreversible magnetization will start to change, and the magnetization will start to spiral in towards the origin. Therefore, we will get asymmetrical loops which is consistent with experimental results [DEL, 2017]. For future works, focusing on magnitude of magnetization could be interesting. Also the model can be extended to take variations of temperature into account. Investigating different types of probability distribution function when averaging over orientation can be studied. I suggest $P(\theta) = \frac{1}{k}\cos^n \theta$ and uniform distribution for ϕ.

References

[JAM, 2017] A Jamali, E Della Torre, E Cardelli, AIP Advances 7, 056010 (2017)

[CAR, 2006] E Cardelli, E Della Torre, E Pinzaglia, IEEE Trans. Magn. 42 (2006) 527.

[DEL, 1996] E.Della Torre and F.Vajda, "Vector hysteresis modeling for anisotropic recoding media," IEEE Trans. Magn., MAG-32, May 1996, pp.1116-1119

[DEL, 1998] E Della Torre, IEEE Trans. Magn. 34 (1998) 495.

[DEL, 1999] E Della Torre, E Della Torre, Magnetic hysteresis, IEEE press New York (1999).

[DEL, 2001] E Della Torre, A Reimers, Physica B. 306 (2001), 72.

[DEL, 2004] G. R. Kahler and E. Della Torre, "Rotational magnetization measurements on magnetic particle recording tape," Physica B, vol. 343, pp. 350–356, Jan. 2004.

[DEL, 2006a] E Della Torre, E Cardelli, IEEE Trans. Magn. 42 (2006), 3126.

[DEL, 2006b] E Della Torre, E Pinzaglia, E Cardelli, Physica B. 372 (2206) 111.

[DEL, 2006c] E Della Torre, E Pinzaglia, E Cardelli, Physica B. 372 (2206) 115.

[DEL, 2015a] E. Della Torre, A. Jamali, H. ElBidweihy, and L. H. Bennett, "Vector Properties of Magnetostriction," J. Appl. Phys. 117, 17D141, 2015

[DEL, 2016] E. Della Torre, A. Jamali, H. ElBidweihy, L. H. Bennett., "Vector Magnetization of a Distribution of Uniaxial Particles," IEEE Transactions on Magnetics, 52, 7300904, (2016)

[DEL, 2017] E Della Torre, A Jamali, E Cardelli (in press)
doi.org/10.1016/j.physb.2017.09.050

[KAH, 2003] GR Kahler, E Della Torre, IEEE Trans. Magn. 39 (2003) 1385.

[KAH, 2005] G. R. Kahler, E. Della Torre, and U. D. Patel, "Properties of vector Preisach models," IEEE Trans, Magn, 41 (2005).

[KAH, 2010] GR Kahler, E Della Torre, E Cardelli, IEEE Trans. Magn. 46 (2010) 21.

[MAY, 2003] ID Mayergoyz, Mathematical Models of Hysteresis and their Applications, Academic press 2003.

[OTI, 1990a] J Oti, E Della Torre, J. Appl. Phys. 67 (1990) 5364.

[OTI, 1990b] J Oti, E Della Torre, IEEE Trans. Magn. 26 (1990), 2116.

[REI, 2002] A Reimer, E Della Torre, IEEE Trans. Magn. 38 (2002) 837.

[WUN, 2009] Wun-Fogle M, Restorff JB, Cuseo JM, Garshelis IJ, Bitar S, IEEE Trans. Magn. 45 (2009) 4112-4115.

[YAN, 2006] L. Yanik, A. Yarimbiyik, and E. Della Torre, J. Appl. Phys. 99, 08D706 (2006).

[STO,1948] E. C. Stoner and E. P. Wohlfarth, *Phil. Trans. Roy. Soc. London A, Math., Phy. Eng. Sci.*, vol. 240, no. 826, p. 599, (1948).

[TAN,2008] C. Tannous and J. Gieraltowski, *Eur. J. Phys.*, vol. 29, no. 3, p. 475,(2008).

[PET,2011] I. Petrila and A. Stancu, , *J. Phys., Condens. Matter*, vol. 23, no. 7, p. 076002, (2011)

[CIM,2013] D. Cimpoesu, L. Stoleriu, and A. Stancu,, *J. Appl. Phys.*, vol. 114, no. 22, p. 223901, (2013).

[VAJ,1993] F. Vajda and E. Della Torre, *IEEE Trans. Magn.*, vol. 29, no. 2, pp. 1532–1537, Mar. (1993).

[STA,1997] Alexandru Stancu, Irinel Chiorescu IEEE TRANSACTIONS ON MAGNETICS, VOL. 33, NO. 4, (1997)

[KUN,2015] A. Kuncser, V. Kuncser. Journal of Magnetism and Magnetic Materials, 395, 34, (2015).

[STO,1991] E. C. Stoner, F. R. S., and E. P. Wohlfarth, IEEE Trans. on Magn., 27, 3475 (1991).

[PET,2011] I.Petrila, A. Stancu, Journal of Physics: Condensed Matter 23, 076002 (2011).